Effect of visual and auditory sensing cues on collective behavior in Vicsek models

Subhradeep Roy*
Department of Mechanical Engineering, California State University, Northridge, California 91330, USA

Masoud Jahromi Shirazi
Engineering Mechanics Program, Virginia Tech, Blacksburg, Virginia 24061, USA

Benjamin Jantzen
Department of Philosophy, Virginia Tech, Blacksburg, Virginia 24061, USA

Nicole Abaid
Department of Mathematics, Virginia Tech, Blacksburg, Virginia 24061, USA

(Received 5 February 2019; published 23 December 2019)

In the present study, we consider two independent sensing modes (auditory and visual) in Vicsek-like models and compare the emergent group-level behaviors in terms of polarization, cohesion, and cluster size. The auditory and visual modes differ in the determination of particle neighbors, which at the level of groups results in higher polarization, lower cohesion, and larger cluster size for the auditory mode relative to the visual. With the increase in average density of the particles, these differences are more pronounced. These differences are due to the fact that these sense modalities robustly generate distinct spatial distributions of the particles. We demonstrate the use of a data-driven approach, called transfer entropy, to distinguish the sensing modalities by considering only a pair of particle trajectories. Such an approach could be applicable to real-world systems, where it may be a challenge to measure the position and velocity of every particle within a swarm.

DOI: 10.1103/PhysRevE.100.062415

I. INTRODUCTION

Collective behavior refers to the emergence of group-level behavior from individual interactions and is observed in both living (e.g., birds [1], fish schools [2], and human crowds [3]) and nonliving systems [4,5]. Collective behavior may arise from purely local rules in the absence of any central coordination, as demonstrated by a variety of models [6–10]. For the popular Vicsek model [11], order spontaneously emerges in systems where particles align their directions of motion to those within a local neighborhood, exhibiting a phase transition from a random disordered state to an aligned ordered state as the intensity of random perturbations of individual velocities decreases or the average particle density increases. Inspired by various features of real-world collective behavior, a number of variants of the Vicsek model have been proposed, for instance, a generalization to three dimensions [12] and consideration of both attractive and repulsive interactions [13]. A restriction of the sensing region (the spatial region determining the neighbors of a particle) from a circular disk to a sector has also been considered in the literature [14,15]. The study is motivated from the fact that the real-world swarms may not have a panoramic view, and the results demonstrate that restricting the sensing region enables the system to attain faster convergence to global alignment [16].

Although it is typically implicitly assumed that pairwise interactions in collective behavior models are mediated by visual cues [14,15,17], there are a number of social species that use auditory cues to at least partly determine their motion, for example, bats and dolphins [18]. This motivates the present study where we investigate a modified Vicsek model in which the particles communicate by independent use of auditory information and compare it to an existing model that uses a visual sensing scheme. One previous study incorporated sound as an additional mode of agent interaction in a Vicsek model [19]. However, it was assumed that sound generation was omnidirectional so that agents can "hear" others regardless of their relative orientation. Outside the Vicsek paradigm, the study in [20] examines more than one sense modality using a network model with consensus and synchronization protocols. However, the network model ignores the spatial distribution of particles and neighbor detection is stochastic. In a study of midges [21], acoustic interactions are introduced via an adaptive gravity model in which the attractive force between particles is assumed to be proportional to sound intensity. Though theoretical models have given limited consideration to auditory cues, a number of empirical studies have provided evidence of animals altering their motion in response to audio cues. For instance, in [22] it was shown that bats navigate by combining signals from multiple sensory modalities including vision and audition. Another study [23] has found a rear-to-front coupling in a flying bat pair, which may indicate that pairs of bats may adjust their flight in response to auditory stimulus.

*sdroy@vt.edu; subhradeep.roy@csun.edu

In the present study, we examine the consequences within the Vicsek paradigm of a purely auditory sensing mode which, unlike [19], restricts the acoustic information emitted by agents to a limited volume around their direction of motion. The auditory sensing implemented in our study emulates a well-characterized directivity pattern that can be observed in ultrasonic beam formation. With directional ultrasound beams, a microphone inside a source's beam can hear the sound, while one at the same linear distance from the source but at a different angular distance may not [24,25]. The present model takes inspiration from biological systems, specifically bat swarms which effectively use this type of directional ultrasound to navigate their environment. We consider in our study an idealized version of the ultrasonic beam and we model it as a sector of a circle. We quantify the resulting collective behavior of simulated groups in terms of order parameters including polarization (group linear momentum), cohesion (a measure of group compactness), and cluster size (a measure of sensory connectedness) [8,26,27]. Measured this way, we observe very different group-level behaviors for a Vicsek model modified to reflect an auditory sensing scheme relative to an existing model that implements a visual sensing scheme. However, it would be difficult to assess whether analogous differences are manifest in real-world groups using these same order parameters. While easy to compute for simulations with perfect state information, they are difficult or impossible to compute when the data for the particles' states are partial or noisy.

To overcome this challenge, we explore the use of transfer entropy, a data-driven model-free method for detecting the dominant direction of information flow [28]. Data-driven methods which include approaches based on information-theoretic entropy have already proved useful in the study of collective behavior, for example, to detect the direction of navigational influence in pairs of animals [23,29,30]. We implement transfer entropy on the data generated from Vicsek models using either auditory or visual sensing schemes and find that transfer entropy effectively distinguishes between these modalities.

The paper organized as follows. In Sec. II we provide details of two models and the relevant order parameters. In Sec. III we provide our simulation results and discuss the effect of average density on group-level behaviors. In Sec. IV we present a model-free method for discriminating sensing modalities using the information from trajectory data. Finally, we draw our conclusions in Sec. V.

II. MODELING SENSING MODALITIES

In this section, we present the general Vicsek framework and formally distinguish visual from auditory sense modalities through the set of sensory neighbors. We then define the order parameters in terms of which collective behavior is described.

A. Vicsek models

We consider N self-propelled particles moving with a constant speed v_0 in a square two-dimensional box of length L with periodic boundary conditions in discrete time. The average density of particles is given by $\rho = N/L^2$. The position and unit velocity vectors of the ith particle at time step k are denoted by $\mathbf{x}_i^k \in \mathbb{R}^2$ and $\mathbf{v}_i^k \in \mathbb{R}^2$, $i \in 1, \ldots, N$, respectively. At every time step, the ith particle assumes the average direction of motion of the neighboring particles with an estimation error characterized by a random noise. Specifically, the heading angle of the ith particle at time step $k+1$ is denoted by θ_i^{k+1} and updates as

$$\theta_i^{k+1} = \tan^{-1}\left(\frac{\sum_{j\in\Lambda_i^k}\sin\left(\theta_j^k\right)}{\sum_{j\in\Lambda_i^k}\cos\left(\theta_j^k\right)}\right) + \Delta\theta_i^k,$$

where Λ_i^k is the index set of the neighbors of the ith particle, including itself, and $\Delta\theta_i^k$ denotes noise and is a random variable uniformly distributed in the interval $[-\frac{\eta}{2}, \frac{\eta}{2}]$, where η is the noise intensity. Based on the heading angle, the velocity vector of the ith particle then updates as

$$\mathbf{v}_i^{k+1} = \cos\left(\theta_i^{k+1}\right)\mathbf{e}_1 + \sin\left(\theta_i^{k+1}\right)\mathbf{e}_2,$$

where $\mathbf{e}_1$ and $\mathbf{e}_2$ are two unit vectors orthogonal to each other. Finally, the position of the ith particle updates as

$$\mathbf{x}_i^{k+1} = \mathbf{x}_i^k + v_0\mathbf{v}_i^k.$$

We use the same update protocol as defined above for both sensory modalities. What distinguishes the two sense modalities is the index set of neighbors Λ_i^k. To model visual sensing, we suppose each particle has a field of vision, modeled as a sector bounded by two radii of length r, symmetric about the individual's current heading. The opening angle of the sector is 2ϕ, where the *sensing angle* ϕ can vary from 0 to π. When $\phi = \pi$ the model reduces to the original Vicsek model, where the interaction neighborhood of a particle is a circle. At each time step, the particles that occupy the field of vision of an individual comprise its set of neighbors Λ_i^k. For auditory sensing, each particle's *acoustic beam* is modeled as a sector of a circle. Similar to the field of vision, the beam has an opening angle 2ϕ, where ϕ can vary from 0 to π, and is also assumed to be symmetric about the individual's current heading direction. The particles, whose beams are occupied by an individual, are defined as that individual's neighbors. In other words, the neighbors of a given particle are all of those particles which it can hear because it is within their acoustic beam. Figure 1 presents the schematic of the two modes of interactions.

B. Order parameters

We define three observables to evaluate the collective behavior: polarization, cohesion, and cluster size.

Polarization is a measure of group alignment given by the average of the normalized linear momentum of the system and can be calculated as

$$P^k = \frac{1}{N}\left\|\sum_{i=1}^{N}\mathbf{v}_i^k\right\|.$$

Polarization ranges between zero and one, where one corresponds to perfect alignment and zero corresponds to a random walk.

Cohesion measures the closeness of the particles with respect to the overall center of mass. To calculate cohesion,

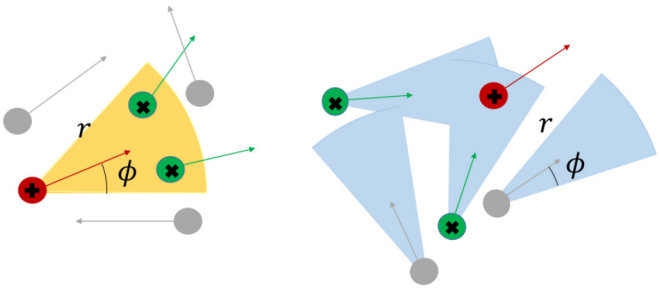

FIG. 1. Schematic showing that the green particles (marked with crosses) are neighbors of the red particle (marked with pluses) based on the sensing scheme used. The gray particles (unmarked) do not qualify as neighbors of the red (plus) particle. Shown on the left is the visual sensing scheme, in which the green (cross) particles lie inside the field of vision of the red (plus) individual and hence are its neighbors. Shown on the right is the auditory sensing scheme, in which the red (plus) individual resides inside the acoustic beam of its neighbors.

we first compute the center of mass of the group as $\mathbf{X}^k = (1/N)\sum_{i=1}^{N}\mathbf{x}_i^k$ and then the relative position of each particle with respect to the center of mass through $\mathbf{r}_i^k = \mathbf{x}_i^k - \mathbf{X}^k$. Cohesion is then defined as

$$C^k = \frac{1}{N}\sum_{i=1}^{N}\exp\left[-\frac{\|\mathbf{r}_i^k\|}{l_a}\right],$$

where $l_a = 4r$ is a scaling coefficient consistent with the study in [8]. Cohesion ranges between zero and one, where one corresponds to a scenario in which all particles are at the center of mass while zero corresponds to the scenario in which all particles are dispersed infinitely far from the common center of mass. Given periodic boundary conditions for a finite arena, a cohesion of zero is impossible.

Finally, *cluster size* corresponds to the size of the largest collection of particles at a given time who are connected to one another by some path in the interaction graph, where the latter is built by drawing an undirected edge from each particle to every one of its neighbors. That is, the cluster size S^k is the size of the largest weakly connected component of the interaction graph at time k. Two particles are therefore in the same cluster if they are connected by a path of interacting particles.

III. DIVERGENT GROUP BEHAVIOR FOR DISTINCT SENSE MODALITIES

The auditory and visual models differ in the determination of particle neighbors. To ascertain the effect of this difference on group-level behavior, we conduct contrasting simulations that differ only in the sensing modality. For these numerical simulations, we set the length of the square box $L = 10$, the radius of the sensing region $r = 1$, the constant speed $v_0 = 0.03$, and the average density of the particles $\rho = 10$. We further vary two control parameters, the sensing angle ϕ and the amplitude of noise intensity η. The initial positions of the particles and their heading directions are randomly assigned within the square box of side length L and in the range $[0, 2\pi]$, respectively, with uniform distributions.

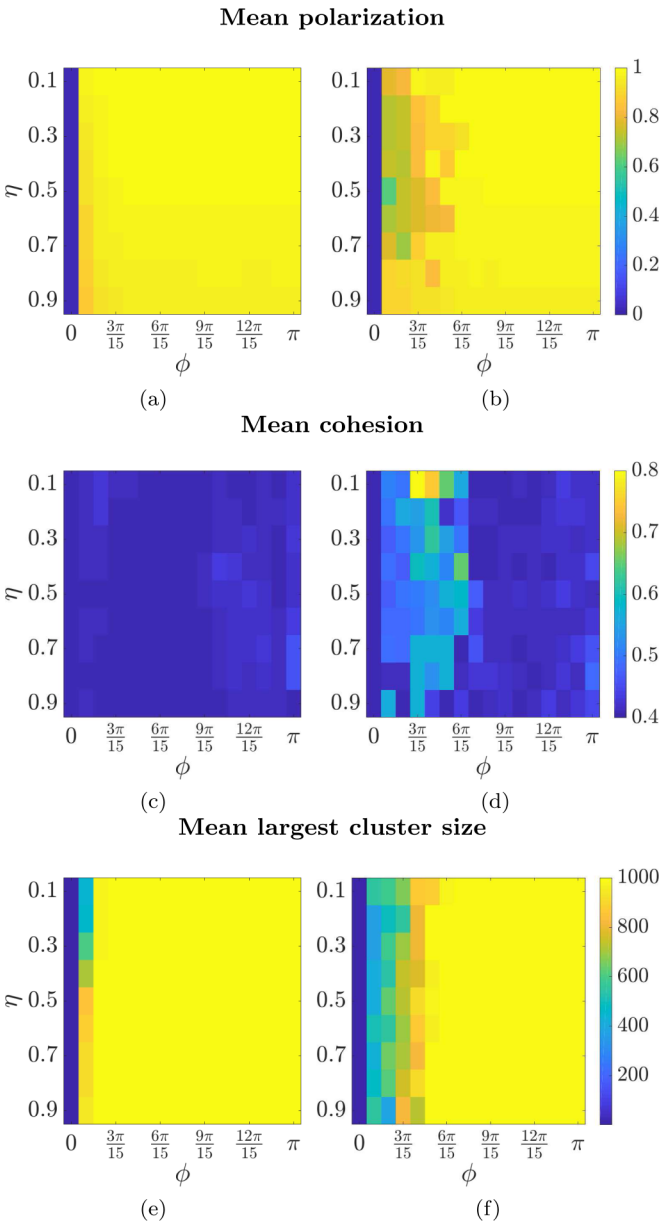

FIG. 2. Order parameters as computed for auditory (left column) and visual sensing (right column) modes when $\rho = 10$.

Though randomly determined, these initial conditions are kept identical for both the visual and auditory simulations. We run our simulations for 50 000 time steps, recording the data only after excluding an initial transient phase of 10 000 time steps. Next we compute the mean polarization, mean cohesion, and mean size of the largest cluster, averaged over the steady state.

Figure 2 shows the results for the order parameters where $\rho = 10$, and η and ϕ are varied. Observing Figs. 2(a) and 2(b), we identify that for both auditory and visual sensing cues, polarization is zero for the special case when $\phi = 0$. This corresponds to the absence of interaction that results in a random walk for the particles for all choices of noise intensity η. On the other hand, polarization reaches the maximal value of one when $\phi = \pi$ for all choices of η and for each of the sensing cues. The special case of $\phi = \pi$ corresponds to the

original Vicsek model, where the sensing neighborhood of the particles is a circle, and hence the neighbor determination mechanism for both the visual and auditory models is equivalent.

However, comparing vertical slices of polarization (columns of constant ϕ in the figures) between auditory and visual sensing modes, we observe a difference when the sensing angle is small. In particular, for the visual sensing mode we observe that the polarization is relatively small at sensing angles of $\phi \leqslant 6\pi/15$ and increases with increasing ϕ. However, in the case of the auditory sensing mode, the particles achieve a polarization of one for all sensing angles $\phi > 3\pi/15$ independent of noise intensity.

The difference in group-level behavior between swarms using auditory and visual sensing cues is also observed in terms of cohesion [Figs. 2(c) and 2(d)] and largest cluster size [Figs. 2(e) and 2(f)]. For example, in the visual mode we observe cohesion is high when the sensing angle is small ($0 < \phi \leqslant 7\pi/15$), as the particles form closely packed clusters. In contrast, for the auditory sensing mode, we observe cohesion is less sensitive to the variation in sensing angle and also that the values are small relative to the visual mode. Again, in terms of cluster size, we notice that the particles form one large cluster for $\phi \geqslant 3\pi/15$ in the auditory sensing scheme, but only for $\phi > 6\pi/15$ in the visual sensing scheme.

A. Effect of the average density on order parameters

The Vicsek model [11] demonstrated a phase transition as the noise intensity decreases or the average density increases. Accordingly, next we investigate the effect of the average density of the particles on the behaviors discussed above. Thus we perform an additional simulation for $\rho = 0.3$. The other system parameters are set as before. The results are shown in Fig. 3. First, we notice that at this lower density, the difference between the two sensing modes in terms of polarization is less pronounced. For both, we clearly see a decrease in polarization from a value of one to near zero with increasing noise when $\phi = \pi/15, \ldots, 8\pi/15$. However, polarization appears to increase slightly faster with respect to ϕ in the auditory mode. With respect to cohesion, differences between the visual and auditory modes are subtle at best; comparing vertical slices, we observe somewhat higher values of cohesion for the visual sensing mode at a given ϕ relative to the auditory sensing mode. However, the pattern of dependence on ϕ and η for either mode is dramatically different from the high-density case. Comparing Figs. 2 and 3, we notice that, unlike in the high-density case, cohesion at low density for both modes increases monotonically with ϕ and attains much higher values at a maximum sensing angle of $\phi = \pi$. With respect to cluster size, we notice that the largest cluster size increases with an increase in the sensing angle. This is because, at small values of sensing angles, the particles fail to interact when the average density is small. However, with the increase in sensing angle the particles begin interacting and the cluster size is primarily dictated by the noise intensity. In particular, as noise intensity increases the particles require larger sensing angle to form one large cluster. This phenomenon is also observed for both sensing modes.

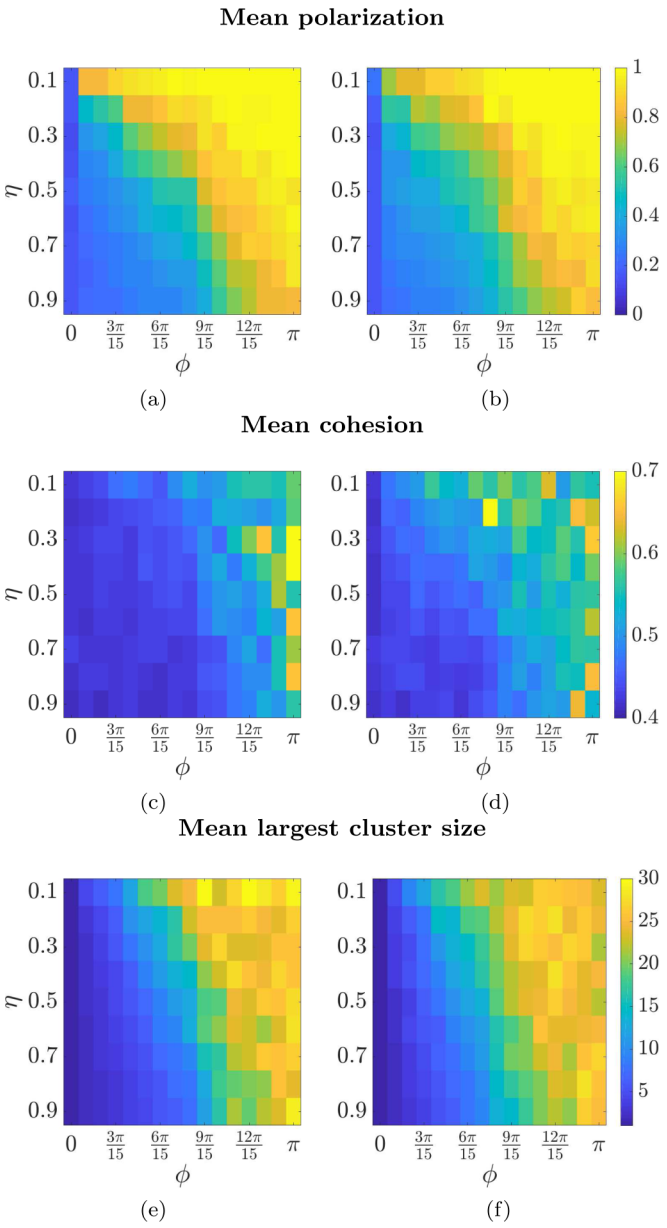

FIG. 3. Order parameters as computed for auditory (left column) and visual sensing (right column) modes when $\rho = 0.3$.

B. Sensing mode determines spatial distribution

In terms of the order parameters considered, distinct sensing modes generate different group-level behavior, especially at high particle density and small sensing angle. The observed differences with respect to cohesion and mean cluster size indicate that particles distribute themselves differently in space depending on sensing mode, and the differences with regard to polarization suggest that patterns of particle orientation differ as well. To characterize the disparate spatial distribution for these two systems, we conduct a new analysis at each density for which $\phi = 4\pi/15$ and $\eta = 0.2$, and all other system parameters are as above. We further divide the square domain into square cells with equal side lengths of one unit. The number of particles in each cell constitutes the cell occupancy. For each time step k in the simulation,

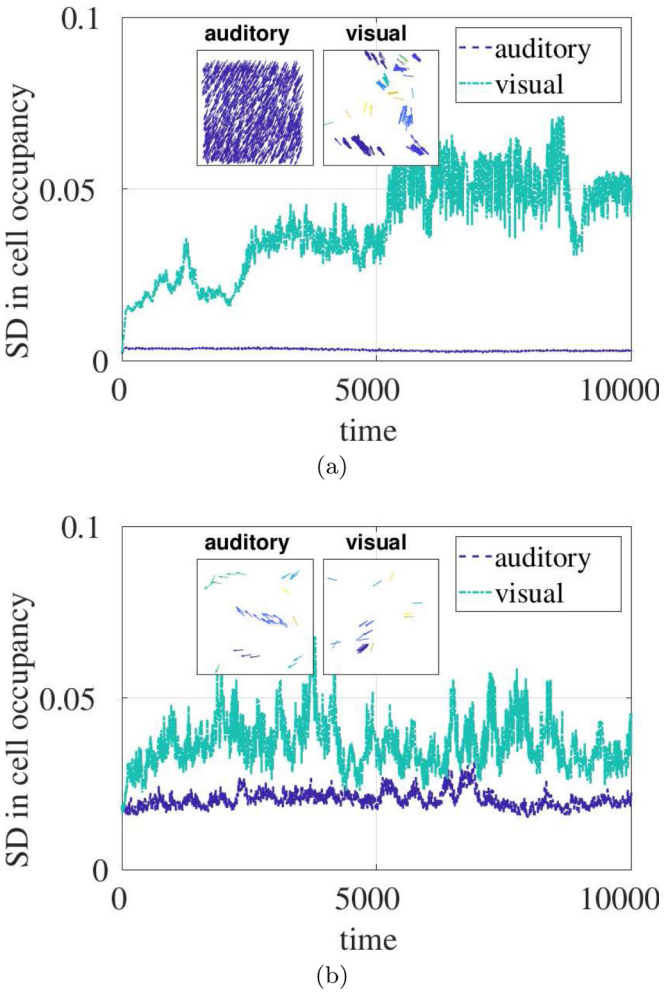

FIG. 4. Standard deviation in cell occupancy for (a) $\rho = 10$ and (b) $\rho = 0.3$.

we compute the standard deviation (SD) in normalized cell occupancy across cells. The normalization is performed by dividing the occupancy in each cell by the total number of particles present in the system. The resulting time series for the high-density case ($\rho = 10$) is plotted in Fig. 4(a). The SD in cell occupancy is small at the beginning (and identical for both modalities) as determined by the uniform random distribution used to set the initial particle positions. For the auditory sensing scheme, the SD in cell occupancy maintains a small value over time, indicating that the particles remain evenly spread over space. This is clear from the inset of Fig. 4(a), which depicts a snapshot of the spatial distribution of the particles at the termination of each simulation. However, the SD increases substantially with time in the visual sensing scheme. This indicates that at later times in the simulation the particles form closely packed clusters, resulting in high cell occupancy values for some cells and zero for the remaining. This is again evident in the inset of Fig. 4(a). These results demonstrate that in the auditory mode with small sensing angle the particles are evenly distributed in space, loosely packed in one large cluster, and perfectly aligned. On the other hand, in visual mode with small sensing angle, the particles form multiple clusters. The particles within the cluster are closely packed and aligned, but all the clusters may not have perfect alignment; hence polarization does not attain value one, but the cohesion increases.

For the low-density case ($\rho = 0.3$), the differences between the sensing modes remain pronounced as is clear from Fig. 4(b), though reduced relative to the high-density case. It is still clear that in the visual case, the SD in spatial occupancy remains higher than for the auditory mode. An explanation for the reduction of the difference is suggested by the inset of Fig. 4. Given the low density, particles in either simulation end up forming spatially disjoint subgroups (clusters). This has the effect of raising the SD for the auditory sense mode. However, within those groups, we see the same pattern of behavior as at high density. Specifically, the auditory sensing agents space themselves in a lattice within a group (e.g., the blue group at the center of the inset), keeping spatial SD relatively low. The visual sensing particles, on the other hand, continue to form compact clusters, driving SD relatively high (though, given that there are fewer agents, the SD cannot be as high as in the high-density case).

C. Distance of closest approach lower for pairwise auditory interactions

We hypothesize that some of this difference may be due to differences in the distance of closest approach (the minimum separation) in pairwise interactions. Specifically, there are interactions in which only one particle senses the other (but not vice versa) where particles operating in the visual sensing mode can approach closer to one another than those in the auditory mode. That is because in the latter case the sensed particle (the particle hearing the beam of the approaching peer) immediately turns away from the oncoming particle. In the visual case, the sensing particle itself adjusts to move into the trajectory of the sensed particle.

To test the hypothesis that such differences in closest approach are systematic and contribute to the observed group-level results, we simulate an isolated pair of particles for each of the two sensing schemes. The initial positions for the two particles are set as $\mathbf{x}_1^0 = (6, 0)$ and $\mathbf{x}_2^0 = (0, 0)$. We further fix the initial heading directions, set $\theta_2^0 = \pi/4$, and vary $\theta_1^0 = \pi/6, \ldots, \pi$. We choose the remaining system parameters as follows: $L = 500$, $r = 3$, $v_0 = 0.01$, and $\eta = 0$. Both simulations are run in the absence of noise ($\eta = 0$), so the trajectories of both particles will be deterministic. This is done to guarantee particle interaction when the initial conditions would allow it and that differences between the simulations are due to the effect of interest rather than random variations in injected noise. Additionally, for each initial θ_1^0, we vary the sensing angle ϕ from $\pi/15$ to π. The simulation is run for 1000 time steps to enable the two particles to attain a steady state and the distance of closest approach is recorded.

Figure 5 presents the difference of the distances of closest approach between the two sensing modes, where we subtract the minimum distance of closest approach for the visual sensing mode from that of the auditory sensing mode. We observe that the difference between the two modes is zero for two scenarios: first, for $\theta_1^0 \leqslant \pi/3$ at all values of ϕ, and second, for $\phi \geqslant 7\pi/15$ at all values of θ_1^0. In the first scenario, the particles never pass through one another's sensing region

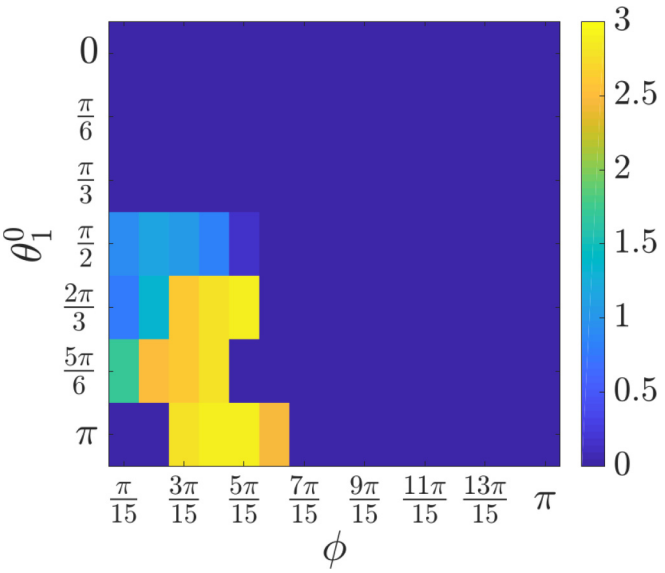

FIG. 5. Difference of the distances of closest approach between auditory and visual sensing modalities for a pair of particles. The positive difference means that in the auditory mode particles maintain a larger minimum separation than in the visual mode.

as the initial heading direction of the first particle is too oblique. In the second scenario, the wide sensing angles mean that both particles sense each other at the maximum possible distance, thus leading to no difference in the two sensing schemes. In all other cases, the difference is positive. Thus the distance of closest approach is sometimes significantly smaller for the visual mode of interaction but never vice versa. This both supports our hypothesis and plausibly accounts for the asymmetry in results seen at the group level at high average density.

IV. DISCRIMINATING SENSE MODALITIES

The results above show that the two distinct sensing modalities lead to significant differences in collective behavior of the simulated swarm at multiple levels of description. The question remains how many collective systems (animal or otherwise) are better represented in terms of an auditory as opposed to visual sensing modality. For the Vicsek models reported here, the differences in sensing modality are detectable in terms of the high-level order parameters. However, computation of these parameters requires perfect information about particle position and momentum over long periods of (simulated) time. This sort of information is impractical to obtain for real world systems. Here we use these modified Vicsek models as a test bed to demonstrate a method for discerning visual from auditory sensing modes using only partial information. This method relies on the notion of transfer entropy.

A. Transfer entropy

Transfer entropy (TE) is based on information theory and measures the amount of directed transfer of information between two time series variables [28]. The expected value of the information associated with the occurrence of an event is referred to as Shannon entropy and is defined as

$$H(X) = -\sum_{x\in\mathbb{X}} \Pr[x]\log_2 \Pr[x], \tag{1}$$

where $\Pr[x]$ is the probability mass function for a time series variable X taking the value x and $\mathbb{X}$ refers to the set containing all possible realizations of X. The TE extends this idea between two time series variables considered as one-step Markov chains to quantify information transfer. For example, given two time series variables X and Y, the TE from Y to X ($T_{Y\to X}$) measures the reduction in entropy of X when conditioned on Y and is defined as

$$T_{Y\to X} = \sum_{\substack{x(t+1)\in\mathbb{X}(t+1),\\ x(t)\in\mathbb{X}(t),\\ y(t)\in\mathbb{Y}(t)}} \Pr[x(t+1),x(t),y(t)] \times \log_2 \frac{\Pr[x(t+1)|x(t),y(t)]}{\Pr[x(t+1)|x(t)]}, \tag{2}$$

where $\Pr[x(t+1)|x(t)]$ and $\Pr[x(t+1)|x(t),y(t)]$ denote the probability of $x(t+1)$ conditioned on $x(t)$ alone and on both $x(t)$ and $y(t)$, respectively; $\Pr[x(t+1),x(t),y(t)]$ denotes joint probability. In case the time series variable Y does not influence variable X, $\Pr[x(t+1)|x(t),y(t)] = \Pr[x(t+1)|x(t)]$, and hence $T_{Y\to X}$ equals zero. In general, $T_{Y\to X}$ and $T_{X\to Y}$ are asymmetric quantities, and by directly comparing them we can identify the dominant direction of influence.

We implement TE using the open-source Java Information Dynamics Toolkit [31]. To estimate the probability mass functions (PMFs) used in the above definitions, we used the Kraskov-Stogbauer-Grassberger method, which uses a dynamically altered kernel width in terms of K nearest neighbors (k_{NN}) that decreases errors in PMF estimation [32].

B. Distinguish sense modalities by analyzing a pair of trajectories using TE

In this simulation study, we consider the use of two sensory modalities independently for a pair of particles and fix their initial positions by placing one particle in front of the other. We place the front particle f at the coordinate (1,0) and the rear particle r at the coordinate (0,0). Both particles start with the same initial heading angle, where $\theta_f^0 = \theta_r^0 = 0$ and constant speed $v_0 = 0.03$. This setup ensures that the interaction direction is from front to rear ($f \to r$) for the visual sensing modality, whereas the direction is from rear to front ($r \to f$) in the auditory sensing modality. The other parameters for the numerical simulation are set as $L = 500$, $\eta = 0.01$, $\phi = 4\pi/6$, and $r = 3$. We run the simulation for 10 000 time steps to generate trajectory data for each particle. As we consider the presence of noise in this set up, the trajectories are stochastic. Thus, we perform a Monte Carlo simulation and generate 20 independent trajectories for the fixed initial conditions and system parameters. From two-dimensional trajectory time series of each particle we compute a one-dimensional curvature-based time series to use as input for TE analysis. We use curvature since it is a measure of a particle's steering and can be used to assess pairwise interaction as, for example, in the study of bats [23,30,33]. Figures 6(a) and 6(b) show the TE results as computed on curvature time series data

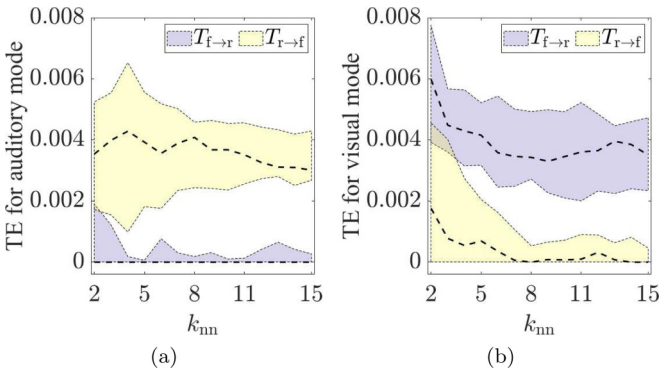

FIG. 6. Implementation of TE on one-dimensional curvature-based time series data considering (a) the auditory sensing scheme and (b) the visual sensing scheme.

for the auditory and visual modalities, respectively. In each panel, TE in the front to rear direction is denoted by $T_{f\to r}$ and TE in the rear to front direction is denoted by $T_{r\to f}$, both as a function of k_{NN}. The central dashed line indicates the median, and the bottom and top edges of the shaded region indicate the 25th and 75th percentiles, respectively.

We notice that TE detects the correct coupling direction for each sensory modality. In particular, Fig. 6(a) shows the TE results for the auditory sensing mode. In this case, the median value of $T_{f\to r}$ is zero for all choices of k_{NN}, whereas the median of $T_{r\to f}$ is strictly greater than $T_{f\to r}$. Thus, TE correctly recognizes that the dominant direction of information transfer is from rear to front. Figure 6(b) shows the TE results for the visual sensing mode, where the median of $T_{f\to r}$ is always greater than $T_{r\to f}$, thus correctly indicating the coupling direction from front to rear.

Thus, TE correctly detects the correct directionality of interaction for each sensory modality. This is an important result, as it demonstrates that TE is a potential tool for detecting the coupling direction between a pair of particles for which the mode of interaction is not known. In addition, these results also confirm that 1D curvature time series may be used as the input variable for such analysis. Thus, in the real world, TE may be a potential tool to detect the sensory modalities used by a pair of individuals. Specifically, if TE detects a rear-to-front coupling, we may infer that individuals use an auditory sensing mode and vice versa.

V. CONCLUSION

Vicsek models have been widely studied in the context of collective behavior. In the present study, we introduced an audition-based sensing modality for a group of self-propelled particles in the Vicsek model and compared the emergent behavior with that of the vision-based sensing modality. Although the auditory and visual sensing modalities differ only in the determination of particle neighbors, they result in disparate group-level behaviors in terms of polarization, cohesion, and cluster size. These group-level differences are more pronounced as the average density of the particles increases. We further demonstrated that the observed group-level differences are due to the fact that these sense modalities robustly generate distinct spatial distributions of the particles. Interestingly, we found that the particles maintain a larger distance of closest approach while using auditory sensing in comparison to that while using visual sensing. Although the group-level differences are reflected in the appropriate order parameters, the effect of distinct sensing modalities may not be obvious while observing only a subset of particles. We demonstrated the use of transfer entropy to distinguish the sensing modality by considering only a pair of particle trajectories. Such an approach could be applicable to real-world systems, where it may be a challenge to measure the position and velocity of every particle within a swarm. This study demonstrates that the sensing modality plays a key role in collective behavior within the Vicsek paradigm, and the results suggest applications involving both biological and robotic swarms.

ACKNOWLEDGMENT

This work was supported by the National Science Foundation under Grants No. 1454190 and No. CMMI-1751498.

[1] I. L. Bajec and F. H. Heppner, Anim. Behav. **78**, 777 (2009).
[2] B. L. Partridge, Sci. Am. **246** (6), 114 (1982).
[3] E. Bonabeau, Proc. Natl. Acad. Sci. USA **99**, 7280 (2002).
[4] V. Narayan, S. Ramaswamy, and N. Menon, Science **317**, 105 (2007).
[5] D. L. Blair, T. Neicu, and A. Kudrolli, Phys. Rev. E **67**, 031303 (2003).
[6] C. M. Topaz, A. L. Bertozzi, and M. A. Lewis, Bull. Math. Biol. **68**, 1601 (2006).
[7] I. D. Couzin, J. Krause, R. James, G. D. Ruxton, and N. R. Franks, J. Theor. Biol. **218**, 1 (2002).
[8] M. Aureli and M. Porfiri, Europhys. Lett. **92**, 40004 (2010).
[9] T. Vicsek and A. Zafeiris, Phys. Rep. **517**, 71 (2012).
[10] A. B. Barbaro, K. Taylor, P. F. Trethewey, L. Youseff, and B. Birnir, Math. Comput. Simul. **79**, 3397 (2009).
[11] T. Vicsek, A. Czirok, E. Ben-Jacob, I. Cohen, and O. Shochet, Phys. Rev. Lett. **75**, 1226 (1995).
[12] A. Czirok, M. Vicsek, and T. Vicsek, Physica A **264**, 299 (1999).
[13] I. Tarras, R. Bakir, A. Hader, M. Mazroui, D. Cambui, and Y. Boughaleb, Sensor Lett. **16**, 123 (2018).
[14] B.-M. Tian, H.-X. Yang, W. Li, W.-X. Wang, B.-H. Wang, and T. Zhou, Phys. Rev. E **79**, 052102 (2009).
[15] Y.-J. Li, S. Wang, Z.-L. Han, B.-M. Tian, Z.-D. Xi, and B.-H. Wang, Europhys. Lett. **93**, 68003 (2011).
[16] M. Durve and A. Sayeed, Phys. Rev. E **93**, 052115 (2016).
[17] X.-G. Wang, C.-P. Zhu, C.-Y. Yin, D.-S. Hu, and Z.-J. Yan, Physica A **392**, 2398 (2013).
[18] J. A. Thomas, C. F. Moss, and M. Vater, *Echolocation in Bats and Dolphins* (University of Chicago Press, Chicago, 2004).
[19] M. J. Shirazi and N. Abaid, Phys. Rev. E **98**, 042404 (2018).

[20] S. Roy and N. Abaid, IEEE Trans. Automat. Contr. **61**, 4063 (2016).
[21] D. Gorbonos, R. Ianconescu, J. G. Puckett, R. Ni, N. T. Ouellette, and N. S. Gov, New J. Phys. **18**, 073042 (2016).
[22] Z. Kong, N. Fuller, S. Wang, K. Ozcimder, E. Gillam, D. Theriault, M. Betke, and J. Baillieul, Sci. Rep. **6**, 27252 (2016).
[23] S. Roy, K. Howes, R. Muller, S. Butail, and N. Abaid, Entropy **21**, 42 (2019).
[24] J. Kuutti, J. Leiwo, and R. E. Sepponen, Technologies **2**, 31 (2014).
[25] Y. Ochiai, T. Hoshi, and I. Suzuki, *Proceedings of the 2017 CHI Conference on Human Factors in Computing Systems* (ACM, New York, 2017), pp. 4314–4325.
[26] M. J. Shirazi and N. Abaid, *ASME 2017 Dynamic Systems and Control Conference, Tysons Corner, 2017* (American Society of Mechanical Engineers, New York, 2017), p. V002T14A010.
[27] C. Huepe and M. Aldana, Physica A **387**, 2809 (2008).
[28] T. Schreiber, Phys. Rev. Lett. **85**, 461 (2000).
[29] S. Butail, V. Mwaffo, and M. Porfiri, Phys. Rev. E **93**, 042411 (2016).
[30] N. Orange and N. Abaid, Eur. Phys. J. Spec. Top. **224**, 3279 (2015).
[31] J. T. Lizier, Front. Robotics AI **1**, 11 (2014).
[32] A. Kraskov, H. Stogbauer, and P. Grassberger, Phys. Rev. E **69**, 066138 (2004).
[33] J. G. Puckett, D. H. Kelley, and N. T. Ouellette, Sci. Rep. **4**, 4766 (2014).